Validation of a full-scale glider crash test model and proposal of cockpit design methods

Marvin Hofmann
marvin.hofmann@tum.de
Chair of Carbon Composites, Technical University of Munich
Munich, Germany

Joscha Löwe
joscha.loewe@tum.de
Akaflieg Munich e.V., Technical University of Munich
Munich, Germany

Marco Tönjes, Christian Pohl, Klaus Drechsler
marco.toenjes@tum.de, christian.pohl@tum.de, klaus.drechsler@tum.de
Chair of Carbon Composites, Technical University of Munich
Munich, Germany

Abstract

This study describes the validation of a numerical sailplane crash model using a full-scale test. First presented is the Mü 32 sailplane design by Akaflieg Munich based on the flight loads and a crash concept. Subsequently, a selection is given of material models for composite, adhesive, and foam materials, which are an appropriate choice to create a numerical crash test model. The composite structure is modeled using strain-rate-dependent behavior. Due to the differential design approach, cohesive connections are of high importance for the behavior of the model. A material model is adapted to obtain stable simulations of sandwich foam cores. A detailed fuselage model is created and a commercial dummy model is integrated. The execution of the crash test, the employed measurement equipment and the evaluation routines are described. High-speed camera footage in combination with binary sensor data facilitate a detailed analysis of the results. Injury criteria are used to evaluate the consequences of the crash for the occupant. Finally, proposals are given for future crashworthy aircraft designs and further numerical loadcase studies.

Introduction

Over the last 10 years, almost 20 persons lost their lives in small powered airplane and sailplane accidents throughout Germany every year [1]. Quasi-static testing of fuselages is the state-of-the-art certification procedure for sailplanes according to EASA (European Union Aviation Safety Agency) CS 22.561 [2]. In order to improve the crashworthiness of sailplanes under hard landing and typical crash conditions, an approach for dynamic crash testing was investigated in the German LuFo V-3 project CraCpit (Crash Cockpit). In addition to the test-driven crashworthiness investigations described by Roger et al. [3] and Waibel [4], this project uses numerical methods to understand the crash load case and optimizes the structure in multiple iteration loops. The crash test validates the modelling approach and the design of the optimized structure The boundary conditions were derived from statistical investigations of sailplane accidents [5, 6], certification regulations, and early simulation results. Also, there was a mutual exchange between the CraCpit project and the German VDI standard 5911 group (Insassenschutz für Kleinflugzeuge) [7].

The present study contains the following sections. The first section describes the **Design of the Mü 32** crash-text aircraft. Next, the **Crash test setup** is described. After showing how the test material data were included in the advanced general-purpose, multiphysics simulation software package LS-DYNA (Section **Material modeling**), the creation of the fuselage model is described (Section **Finite-element model creation**). The

This article has been reviewed according to the *TS* Fast Track Scheme.

results of the full-scale crash test compared to the simulation model, including an analysis of the injury risk for the pilot, are presented in Section **Results of test and simulation**. The Section **Numerical loadcase studies** presents results from simulations with different boundary conditions. Based on the findings a **Proposal for cockpit design methods** for future applications is given. Finally, a summary of the results is given in the **Conclusion** section.

Design of the Mü 32

The design of Akaflieg Munich Mü 32 is based on (a) an analytical flight load dimensioning along with (b) the integration of a crash concept with the canopy frame reinforcements and keelbeams including (c) a lay-up-optimized nose cone section. Figure 1 shows a schematic cross-section of the canopy reinforcement structure introduced by Kudla [8]. The crash concept was inspired by the idea of Schuster and Wolf [9], who introduced two beams extending along the longitudinal direction below the cockpit (keelbeams). A foam core combined with up to 12 unidirectional carbon fibre layers was used to reinforce the cockpit section. Carbon-aramid fabric was applied in the outer- and innermost layers for splinter protection.

The layup of the fuselage and the crash beams was optimized with LS-OPT using a simplified model of the nose cone [10]. The objective of the optimization was to control the crash kinematics of the fuselage, aim for continuous energy absorption, and minimize the accelerations on the pilot. As the ply design is optimized for an impact angle of 45°, an angle of 45° for the ply boundaries referred to the longitudinal axis (X-axis) of the glider was chosen as illustrated in Fig. 2. Figure 3 shows the laminate thickness of the global fuselage laminate structure and the laminate of the upper keelbeam reinforcement structure over the X-position of the fuselage starting at the nose cone of the aircraft. The thickness of the global fuselage laminate was measured along the centerline of the upper and lower keelbeam. The resulting design features a progressive increase in the number of layers from the nose toward the rear of the cockpit allowing progressive failure (crushing) of the nose cone. Behind the cockpit opening the thickness of the composite structure is reduced.

Crash test setup

On July 26, 2022, two full-scale crash tests were successfully completed by Akaflieg Munich and Akaflieg Hannover together with Technical University of Munich and Leibniz University of Hannover. The CraCpit project used synergies with the NaSiCo (Nachrüstung Sicherheitscockpit) project which investigated a reinforcing structure which can be retrofitted into existing gliders. In the present study, only the CraCpit test is shown.

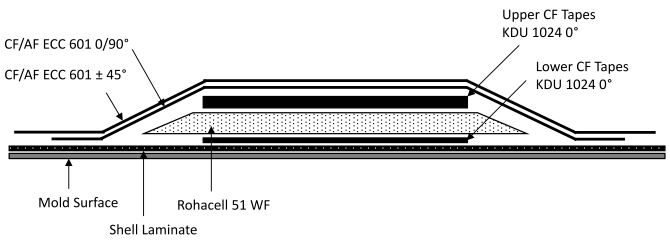

Fig. 1: Schematic side view of canopy frame reinforcements.

The impact was designed to occur with a velocity of 15 m/s and at an angle of 45° between the barrier and the longitudinal axis of the glider. In addition, a 5° angle of sideslip was defined in accordance with EASA CS 22.561 [2]. These test parameters are recommended as a baseline for future investigations of the crashworthiness in gliders and small powered airplanes.

A drop test was chosen as a test setup. Energy was introduced into the system as potential energy, which was almost entirely converted into kinetic energy during the drop of the fuselage. An asphalt runway surface represented the rigid barrier. As the crash test could only be performed once due to the enormous time and resource expenses, it was highly important that the crash setup was well-prepared. Table 1 shows that all impact conditions were satisfied within a reasonable range. It can be noticed that the aircraft was rotated around the longitudinal axis prior to the crash. The rotation resulted in an unexpected impact of the wing substitute mass on the ground after the first impact. The test impact conditions were integrated into the simulation model to maximize the comparability between the test and the simulation.

The test setup consisted of a rigid steel crossbeam lifted by one crane and fixed to the ground with four ropes. This crossbeam acted as a fulcrum, around which the fuselage was allowed

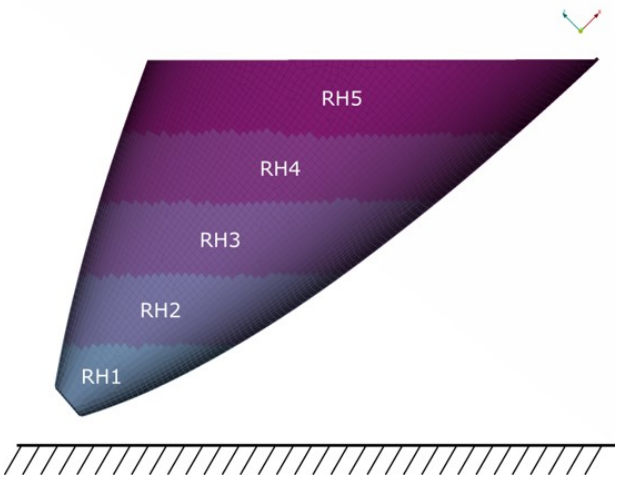

Fig. 2: Laminate partition of the nose cone section.

Table 1: Defined and measured impact conditions.

Impact condition	Defined	Measured
Impact angle	45.0°	45.0°
Impact velocity	15.0 m/s	14.6 m/s
Sideslip angle	5.0°	7.8°

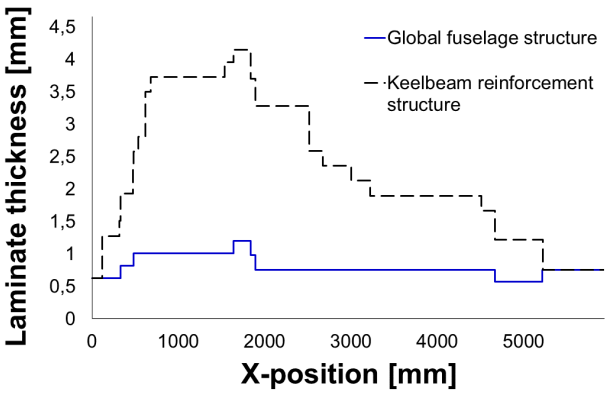

Fig. 3: Laminate thickness of the global fuselage structure and the upper keelbeam reinforcement structure over the X-position of the fuselage.

to swing. A second crane lifted the crash fuselage. The position of the fuselage and swing axis relative to the ground, in combination with defined rope lengths, determined the boundary conditions. Figure 4 shows a sketch of the test setup [11]. The implementation of the test setup and the test site at the Flugwerft in Oberschleissheim are shown in Fig. 5. This setup is less accurate than state of the art crash sleds used in the automotive industry, but it allowed the fuselage to move in all degrees of freedom after impact, yielding a more realistic test scenario.

For validation and transfer into the simulation model, the boundary conditions of the test needed to be captured accurately. Therefore, extensive and trustworthy measurement equipment was included and external experts from many contributing companies were called in. A Hybrid III (H3) 50-percentile male dummy with sensors for displacement, force and acceleration was used to determine the severity of the impact for the pilot. The dummy can be seen in Fig. 6 prior to the crash test. The same type of dummy was also utilized in the simulation model such that a high-level comparison between the test and the simulation as well as detailed analyses of the injury risk for the pilot could be conducted. An Inertial Measurement Unit (IMU), belt force sensors, high-speed cameras, and strain gauges were used to gather additional data. Eleven strain gauges were placed on the inside of the keelbeam supporting structure. They were placed at the front of the aircraft behind the area where crushing of the nose cone was expected. The signals added little informative value to the analyses due to low amplitudes combined with a poor signal quality and were therefore left aside for the validation process. A common trigger signal allowed for data synchronization.

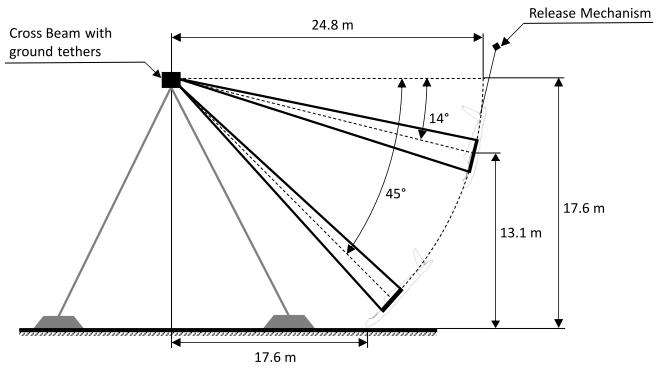

Fig. 4: Schematic side view of the test setup.

Material modeling

As part of the CraCpit project, a material database was established systematically following the building block approach illustrated in Fig. 7: The relevant material data were gathered from literature or coupon-level experiments. The latter were partly carried out on the Split-Hopkinson bars at the Chair of Carbon Composites, Technical University of Munich to characterize the material response under elevated strain rates where necessary. The generated material database can be provided by the author and the Akaflieg Munich e.V. It contains data from three composite, one adhesive material, and one structural foam: carbon-epoxy systems Carbon-Band KDU 1024 - Hexion LR

Fig. 5: Test setup at Flugwerft Unterschleißheim.

Fig. 6: 50th percentile male dummies prior to the crash test.

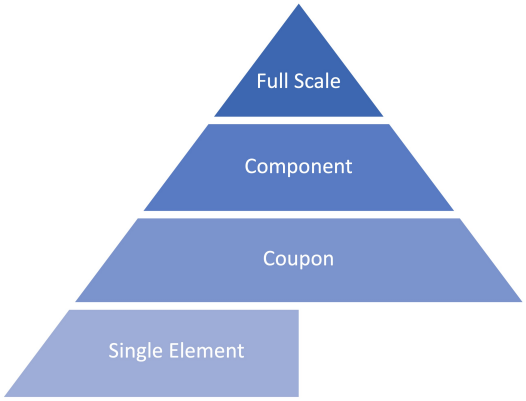

Fig. 7: Building-block approach.

285 / LH 287 and ECC Style 452 - Hexion LR 285 / LH 287, carbon-aramid-epoxy system ECC Style 601 - Hexion LR 285 / LH 287 and resin thickened by cotton flocks and Aerosil based on Hexion LR 285 / LH 287. In the following, the utilized material modeling is presented, which builds the basis for accurate and stable simulations.

Composite materials

One focus of the research project was accurately modeling the composite structures in LS-DYNA [12]. Therefore LS-DYNA material model *MAT_LAMINATED_COMPOSITE_FABRIC (*MAT_058) was chosen. *MAT_058 is a constitutive-continuum damage model proposed by Matzenmiller et al. [13]. The classical lamination theory assumes a plane stress condition for shell elements and linear-anisotropic elasticity. Hashin's four to five failure criteria are optionally included [14]; otherwise, maximum stress criteria can be applied. The material model was implemented in LS-DYNA by Schweizerhof et al. [15]. Pohl et al. proposed a framework to consider fracture toughnesses in the material model [16]. Three-point bending and crushing tests of Omega-shaped profiles were performed to validate the material cards. Strain-rate-dependent material characteristics were included and delamination failure was investigated in crushing validations on Omega-shaped profiles with up to 8 layers of single-ply shell elements. Cohesive elements connected the individual layers. These discrete-ply models also were evaluated in another study by Pohl et al. [17]. However, the predictive improvements of the detailed models were comparably minor at the cost of increased modeling effort and simulation run times, such that the full-scale structure was set up as a single-shell model instead.

Adhesive joints

The fuselage structure is based on the differential design approach. Therefore, modeling adhesive joints between single components has a significant effect on the damage prognosis of the fuselage model. The adhesive connections were represented by cohesive element formulation ELFORM 20 in combination with material model *MAT_COHESIVE_MIXED_MODE_ELASTOPLASTIC_RATE (*MAT_240). The model was developed by Marzi et al. [18]. Strain-rate-dependent fracture toughnesses and yield strengths using a bi- or trilinear traction-separation law were implemented. For yield and damage initiation, mixed-mode loading also might be considered, but is beyond the scope of this study. Component tests were performed and validated in component simulations to include the failure behavior of the adhesive. Figures 8a and 8b show simulation models on the component level for three-point bending tests and crushing simulations performed by Königbaur [19]. Strain-rate-dependent data were not collected for the cohesive material. Therefore, an equivalent strain-rate-response, as for the shear failure of KDU1024 - Hexion LR 285 / LH 287, was assumed and implemented for the through-thickness strength values as the materials share the same epoxy resin. This approach was also used by Lißner et al. [20].

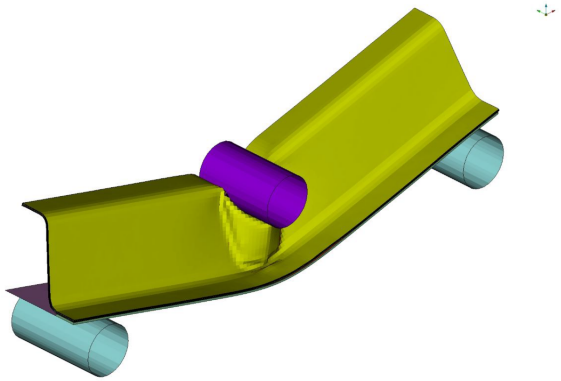

(a) 3-point bending

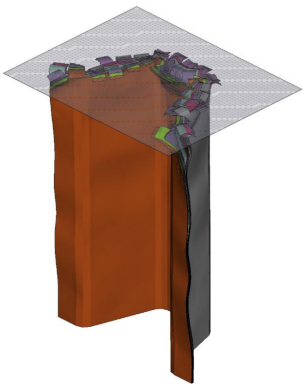

(b) Crushing

Fig. 8: Simulation of composite Omega-shaped profile.

Foam material

Essential structural elements of the crash concept are the keel-beams, which run along the longitudinal axis of the fuselage. They primarily support the loads with unidirectional carbon fiber layers. The crash beam concept is based on a sandwich design that uses low-density structural foam Rohacell IG-F 51. Detailed material data were taken from literature and included in the material model *MAT_DESHPANDE_FLECK_FOAM (*MAT_154) using a solid element formulation ELFORM 1 [21]. *MAT_154 is a three-dimensional continuum damage model for structural isotropic foams originally defined by Deshpande and Fleck and implemented in LS-DYNA by Reyes et al. [22]. The model facilitates a non-linear stress-strain response with plateauing stress, subsequent strain hardening, and optional failure stress or strain definitions. During the setup of the full-scale simulations, the foam material continuously caused instabilities and error terminations. To achieve stable simulations, the following settings were applied: Based on the gathered material properties, failure principal stress PFAIL was defined to be 1.9. Also, an analytical solution scheme instead of a numerical one (DERFI = 1) benefitted numerical stability. After these modifications, the extended foam model showed stable behavior and plausible results for different load cases.

Finite-element model creation

The full-scale crash simulation model was created in the environment of the preprocessor ANSA [23], LS-DYNA was used as a solver, and post-processing and detailed analysis were carried out with META [24]. The following subsections provide descriptions of the modeled entities, contact, hourglass settings, and details regarding the computation on a high-performance cluster.

Fuselage modeling

Shell elements were used primarily to model the fuselage structure. Solid elements were applied for core modeling and the dummy model only. The individual parts were joined by structural bonds made up of cohesive zone elements. The model was meshed with a 6 mm nominal element size. However, for the cohesive zone elements, an element length of 4 mm was used to increase the resolution of the fracture-process zone.

Mass modeling

The mass and center of gravity of the equipped sailplane, including the H3 50-percentile dummy and wing-substitute mass, were measured before the crash and integrated into the final model. As the support structure of the wing-substitute mass came in contact with the ground during the impact, it was modeled with shell elements. Additional balancing masses were used in the test setup to adjust the weight and center of gravity to agree with flight conditions. These additional masses were represented by point masses in the simulation model. This detailed modeling approach reduced to a minimum any deviations between the hardware fuselage and its numerical mode.

Dummy and seatbelt integration

In the crash setup, a five-point safety harness was used. The position of the crash dummy in the cockpit was reproduced in the simulation model. The virtual dummy was positioned with the articulation function in ANSA. A seatbelt tool macro included in ANSA allowed for a very efficient model creation: The tool required a start node, an end node, and a body to be draped onto. In the seatbelt areas not contacting the dummy, a 1D element representation was chosen, whereas shell elements were created in the area of contact with the dummy body as illustrated in Fig. 9. The material model *MAT_SEATBELT (*MAT_B01) was used for the 1D elements and the material model *MAT_FABRIC (*MAT_34) for 2D elements. Both models are standard LS-DYNA material models using a linear modeling approach [12].

Rope suspension and barrier representation

The polyester ropes were modeled in the simulation because they significantly influence the fuselage's kinematics after the first impact. In order to reduce numerical oscillation of the ropes, a damping coefficient (DAMP) of 1 was used. Due to runtime efficiency considerations, no gravitational force was applied to the fuselage. The friction coefficient (FC) between the composite fuselage and the runway was not determined experimentally. In order to evaluate the friction influence, the FC was varied from 0.3 to 0.4 in a parameter study, which is not shown here. The variation did not significantly affect the crash kinematics, which is why a FC of 0.3 was defined for the rest of the study.

Contact and hourglass definitions

A simple but well-defined contact formulation is vital for a stable and physically valid crash model. Only one global contact definition was used to prevent contact definitions from counteracting each other. *CONTACT_..._TIED_... definitions were introduced to model connections between parts, which were of little interest to the crash. Cohesive elements were connected to

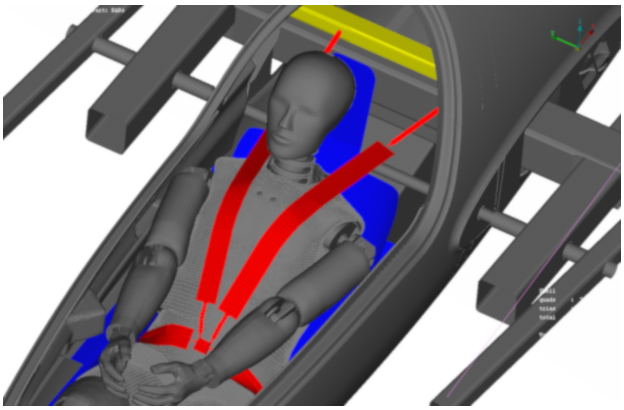

Fig. 9: Seat (blue) and seat belt (red) in the simulation model.

the substrates by TIED contacts as well to stabilize the simulation of the sandwich foam core. Additional pre-defined contacts were only used inside the dummy model.

In order to minimize non-physical element deformation, possible causes for the so-called hourglassing were ruled out during the model creation. Shell elements replaced the original modeling using *RIGIDWALL. Thus, possible non-physical processes were easier to detect visually. Furthermore, point masses and rigid elements were also prevented from entering the rigid barrier, which had posed an error source in early-phase simulations. The energy progress was monitored as well. Due to reduced element formulations in the model, hourglassing effects needed to be controlled individually depending on the properties.

Computation

Simulations were performed with LS-DYNA version R13 MPP double-precision on 28 Intel Xeon E5-2690 v3 (2.6 GHz) cores of the Leibniz Supercomputing Center in Garching, Germany. The final validation model with 1.2 million elements required 88 hours runtime to compute the complete crash up to 450 ms at a time step of 0.58 μs. Figure 10 shows an overview of the model.

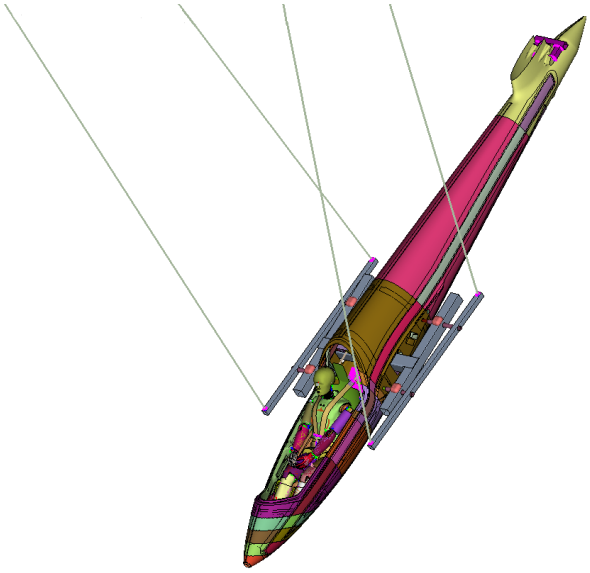

Fig. 10: Overview of the fuselage simulation model.

Results of test and simulation

The crash test and simulation model results are analyzed in parallel. At first, recordings of the high-speed cameras and 3D plots of the simulation are compared. As a second step, the visual impressions are enhanced by comparisons of binary sensor data such as force and acceleration results. Also, these data are further investigated to evaluate the injury risk for the pilot based on injury criteria from literature.

Visual comparison

The model is compared with the high-speed camera recordings by synchronizing test and simulation footage to identify apparent deviations. The subfigures in Figs. 11 to 13 show a synchronized image sequence from 0 to 450 ms with an interval of 50 ms each. A side view and a front view are shown for each interval. Note that the test article is the fuselage with the lighter shade, while the simulated fuselage has a darker shade.

The first five pictures show the initial impact from 0 ms to 250 ms. The movement of the dummy in the simulation is similar to the dummy kinematics in the test. The point at which the front ropes are no longer under tension is nearly identical for the test and numerical model. After the initial impact, a rebound occurs. The residual elasticity of the nose structure evokes an upward springback of the fuselage. The side view shows this behavior is more pronounced in the test than in the simulation. Overall, the test fuselage is further away from the ground than in the simulation. After 250 ms, it can be observed that the crash fuselage has already traveled a longer distance than the model. This can be attributed to the longer contact duration between the fuselage and the barrier caused by the reduced residual stiffness of the fuselage in the simulation. Interestingly, the stiffness deviation can in turn be explained with the implementation of elastic softening in the continuum damage model. This is a drawback of *MAT_058, also reported by Xiao et al. [25]. More advanced material representations considering material plasticity, e.g., proposed by Thomson et al. [26], could be applied to rule out this unintended unloading behavior.

The rear ropes of the model become loose about 250 ms after the first impact, whereas the rear ropes of the test setup are still under tension. This deviation increases over time. The tail of the test fuselage hits the ground earlier than in the simulation. The motion of the dummy continues to show strong similarities between the test and simulation. However, the time offset of the second impact (tailslap), also affects the motion of the dummy. During the tailslap, the difference in the distance traveled becomes even more evident. Again, this effect is created by the reduced residual elasticity of the composite material model. The front view also reveals that in the simulation model, the fuselage rotates more around the longitudinal axis toward the end of the crash. Overall, the Finite Element (FE) model is able to predict the hardware crash kinematics to a large extent. Remaining deviations can be mainly explained by the applied material model.

The simulation shows a good prediction of the structural integrity: Figs. 14a and 14b show the substantial equivalency of the nose cone damage in the simulation and the test. Also, the cohesive model offers a good prediction of the damage pattern in the test. The revision of the cohesive material data and the finer mesh size was of high importance: they increased the similarity of the results between the test and the simulation model, especially regarding local damage to the cohesive structure. In future use of the provided cohesive model, it has to be considered that the strain-rate-dependency needs to be validated even if the results appear reasonable. Specific details of the test, such

0 ms side view

0 ms front view

50 ms side view

50 ms front view

100 ms side view

100 ms front view

150 ms side view

150 ms front view

Fig. 11: Superimposed side and front views of the fuselage crash between 0 ms and 450 ms.

200 ms side view

200 ms front view

250 ms side view

250 ms front view

300 ms side view

300 ms front view

350 ms side view

350 ms front view

Fig. 12: Superimposed side and front views of the fuselage crash between 0 ms and 450 ms (continued).

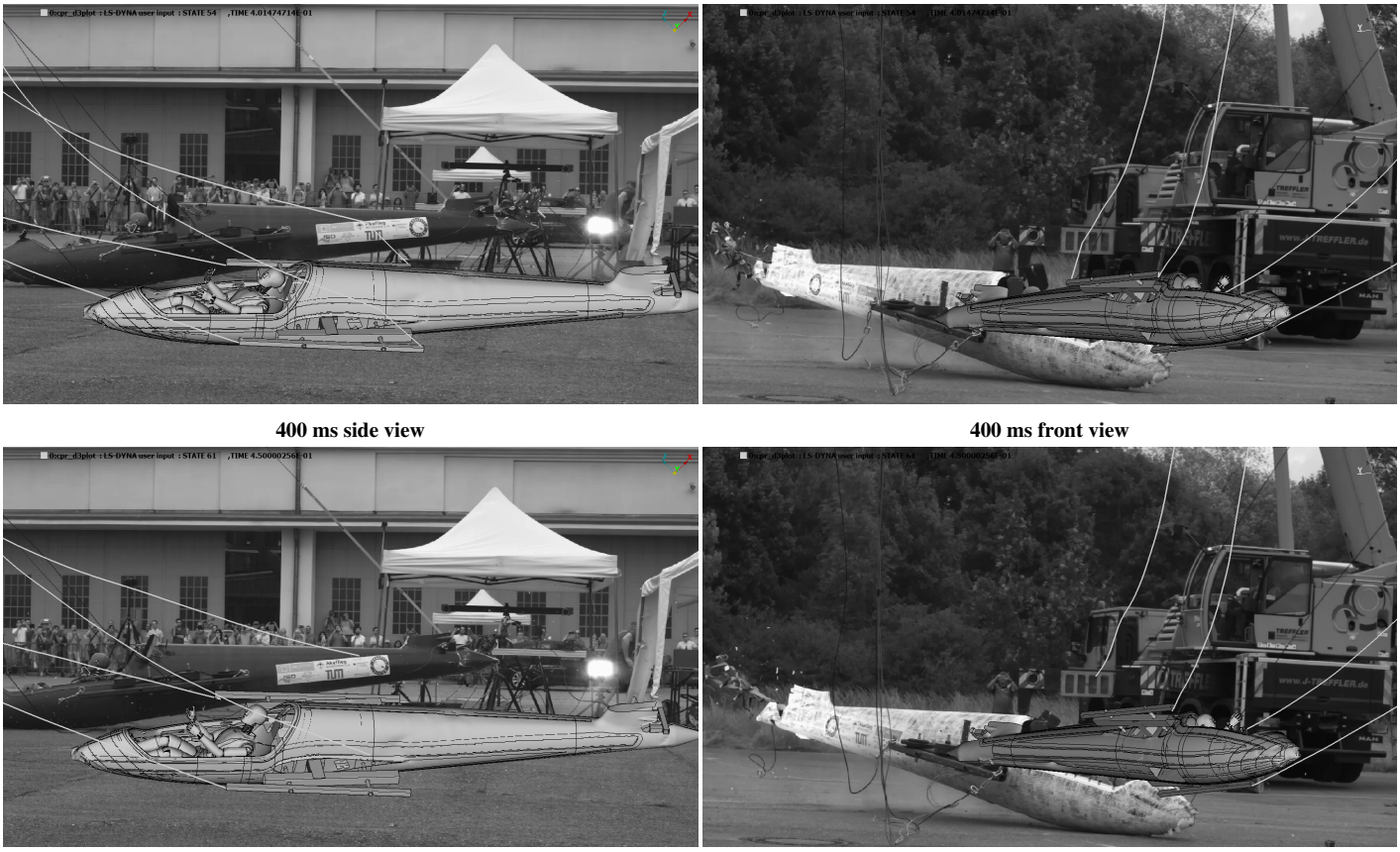

400 ms side view **400 ms front view**

450 ms side view **450 ms front view**

Fig. 13: Superimposed side and front views of the fuselage crash between 0 ms and 450 ms (continued).

(a) **Crash test**

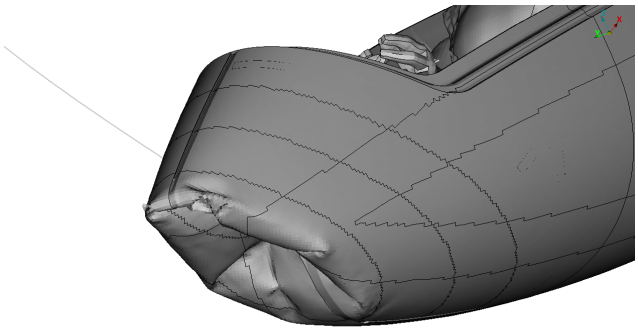

(b) **Simulation model**

Fig. 14: Damage pattern of the nose cone in simulation and test after the crash.

as the local failure of the canopy frame, also can be observed in the simulation.

Accelerations and Eiband curves

In addition to the purely visual evaluation of the crash test, binary data are compared for further analysis. Accordingly, in Figs. 15 through 18 all simulation data are marked by solid curves and all test data by dashed curves. The accelerations were recorded by the Inertial Measurement Unit (IMU), which was mounted close to the center of gravity of the fuselage.

Accelerations

Figure 15 shows the accelerations over time in the IMU coordinate system from the simulation model and IMU crash test data. In each case, Butterworth filters with a cut-off frequency of 50 Hz were used to smoothen the signals [27]. For each curve, initial peaks occur at roughly the same time. The first acceleration peak is reproduced well by the model. The three acceleration component curves show a substantial similarity between test and simulation for the first impact. Timing and amplitude are very comparable and start to deviate from each other only during the rebound. However, the peaks of the second impact

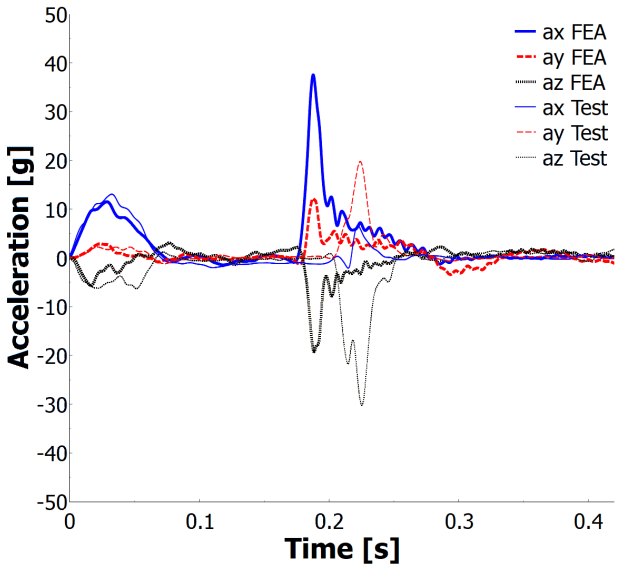

Fig. 15: IMU acceleration in test and finite element analysis (FEA) model.

differ significantly. The peaks of the tailslap occur about 30 ms before the peaks of the test in the modeling. Considering the visual analysis, this effect can be explained by the time offset of the second impact produced by the stronger lift-off of the fuselage in the test. Also, it should be noticed that the second acceleration peak in the x-direction is more significant in the simulation model than in the test. The fuselage model is decelerated more strongly at this point, which is in line with the increased contact duration. Furthermore, it can be observed that the rear ropes in the model have lost their tension earlier. This also can affect kinematics because the ropes exert a force. On the other hand, the accelerations of the second impact in the y- and z-directions (vertical and lateral aircraft axes, respectively) are slightly higher in the test than in the model. This can be attributed to the more pronounced buckling of the rear fuselage structure in the FE model. The accelerations are distributed differently in the three directions between test and simulation.

Eiband curves

To evaluate injury criteria, the time for which the body is exposed to a certain load is considered [28]. In addition to exposure time plots, local forces and accelerations are analyzed over time. That way, deviations between the test and simulation can be clearly identified. Eiband curves provide a first estimate of the expected injuries [29, 30]. Subsequently, local injury criteria are considered. Finally, the expected injuries are evaluated on the dummy and summarized based on a graphical overview.

Eiband curves can be used to perform an initial assessment of injury severities based on acceleration data. These curves use the previously evaluated accelerations and transform their time

evolution into summarized exposure times. Eiband curves facilitate a conservative evaluation at each acceleration level. Detailed Eiband injury risk curves exist in the literature; these show which loads human bodies can be exposed to without being injured. Additionally, limit curves were defined with acceleration levels above which moderate or serious injuries should be expected [31, 32].

Figure 16 shows the acceleration data in the x-direction and the corresponding Eiband curve for negative accelerations over exposure time. These curves are based on the accelerations shown in Fig. 15. The simulation shows higher accelerations than the test up to exposure times of 20 ms. The reasons for this have already been described in the context of the analysis of the acceleration data. Nevertheless, test and simulation are clearly below the limit curve for minor injuries. Therefore, no injuries are expected according to this criterion. Similarly, accelerations in z-direction are evaluated over exposure time. The simulation and test data are mainly equivalent. It can be seen in Fig. 17 that the Eiband curve was slightly exceeded for moderate injuries. This increases the risk of minor injuries in the pilot's spine.

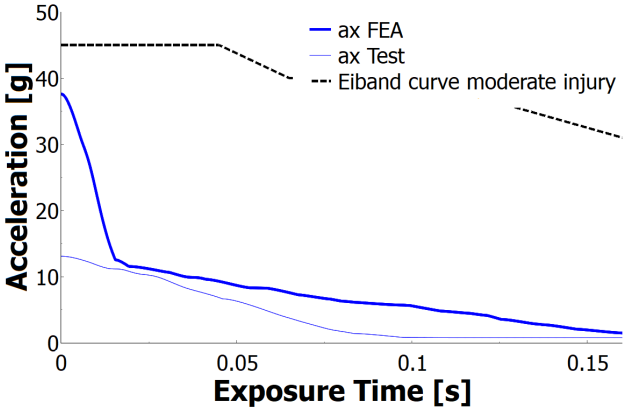

Fig. 16: Eiband curve in x-direction test and FEA.

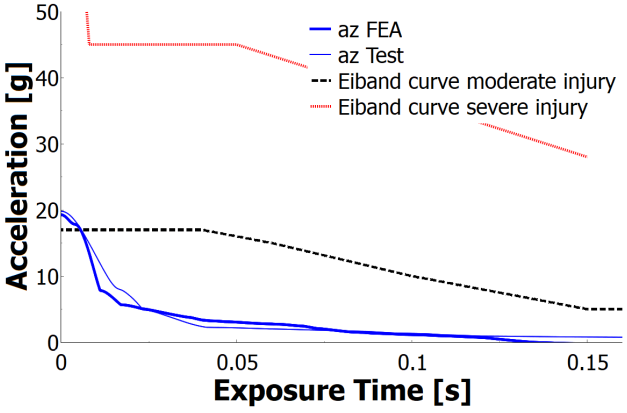

Fig. 17: Eiband curve in z-direction test and FEA.

Head Injury Criterion

The Head Injury Criterion (HIC) describes the injury risk for the head based on accelerations in the dummy's head and their duration. Equation 1 shows the exact calculation of the non-dimensional HIC value according to Hutchinson et al. [33]. The observation period is considered to be 15 ms or 36 ms. In the context of the present study, the following HIC value normalizing the acceleration $a(t)$ over 36 ms from t_1 to t_2 is used (HIC36).

$$HIC_{36} = \left[\frac{1}{t_2 - t_1}\int_{t_1}^{t_2} a(t)dt\right]^{2.5}(t_2 - t_1) \tag{1}$$

The diagram in Fig. 18 shows the head acceleration of the test and simulation. The first acceleration peak is described well by the simulation. This peak is higher than in the test and increases more abruptly due to the missing belt pretensioning. The test has a second acceleration peak at 300 ms, which is less pronounced in the model. The test and numerical HIC36 reach a maximum value of approximately 70 during the crash event, far below the critical value of 1000. According to the HIC severity differentiation by Mackay, even the probability of minor head injuries is very low [34]. The critical HIC values are reached at different times. This is not intuitive, but is justifiable due to the lack of a second peak in the simulation. Besides, the head acceleration must not be greater than 80 g over 3 ms [35]. This value was not exceeded either.

Neck Injury Criterion

The Neck Injury Criterion (NIC) was evaluated in the longitudinal and axial direction. The accumulated force over duration did not exceed the given injury criteria curves, such that no injuries in the neck of the occupant were expected. Therefore, the NIC diagrams are not shown here.

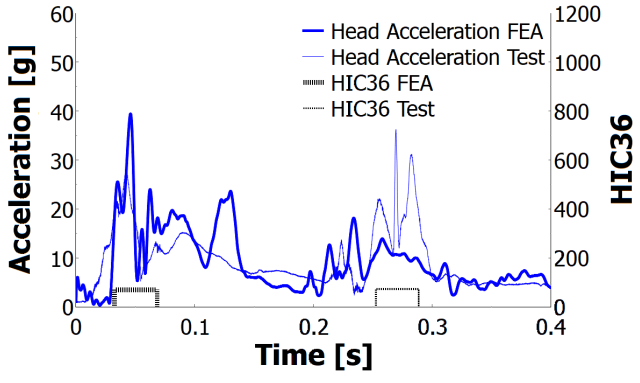

Fig. 18: Head acceleration and Head injury Criterion normalized over 36 ms (HIC36) for test and FEA.

Lumbar Load Criterion

The injury severity of spine injuries can be determined using the Lumbar Load Criterion (LLC). The maximum limit value for compression forces onto the spine is 6672 N [36]. In Fig.19, the force on the lumbar spine is described over the exposure time. The critical LLC value was just undershot in the test. The load calculated by the simulation model lies overall above the test's load curve and exceeds the limit value. Therefore, a high risk of injury to the lumbar spine is expected. However, it should be mentioned that no energy-absorbing cushion was used in the crash test to facilitate the comparison with the simulation model. It has been shown by Segal [37] that energy-absorbing foam could reduce the risk of lumbar injuries in sailplane accidents.

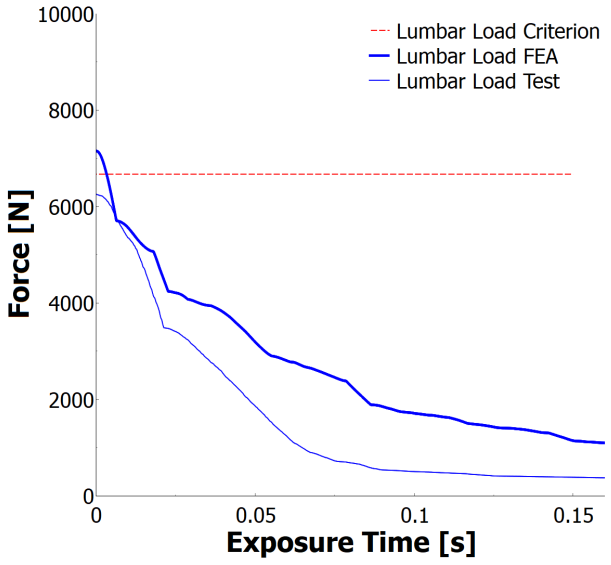

Fig. 19: Lumbar Load Criterion for test and FEA.

Seat belt forces

Figure 20 shows the recorded forces of the seatbelt during the crash test in comparison with the simulation for both sides of the shoulder harness. The curves of the seatbelt force during the test show a pretension of 0.5 kN before the actual peaks around 0.1 s. In the simulation model, no pretension was applied, which also can be observed from these curves. The peak in the simulation model is delayed around 20 ms in comparison with the test. The peak force of the FEA reaches a maximum of 3.5 kN for the left seatbelt, whereas the left belt in the test shows a peak of 1.5 kN but for a longer period. This effect can be explained by the lack of pretension in the seatbelt. Similar characteristics are found for the right seatbelt.

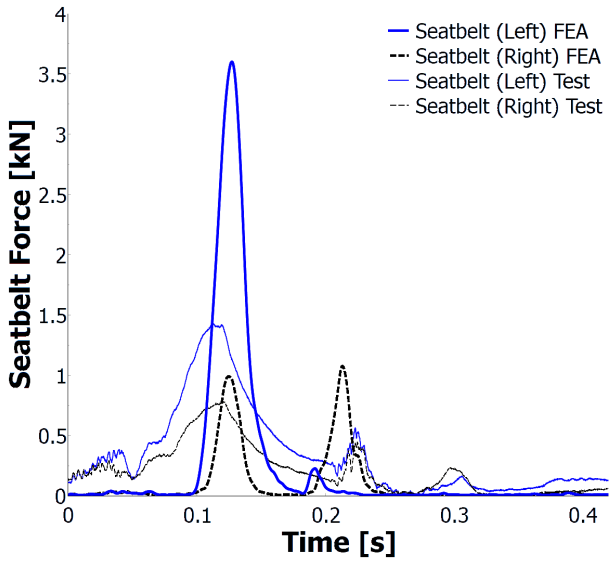

Fig. 20: Forces of the seatbelt in test and FEA.

Injury overview

The injury severity is visualized in Fig. 21 using an illustration of the dummy. The colors of the body parts show the respective severity of the injury. In this context, green color means that no significant injury is expected, whereas yellow indicates a risk of mild to moderate injury. As soon as a criterion is significantly exceeded and injuries are expected, the corresponding body part is colored in red. This figure is also used to compare the pilot's injuries under varying loadcases.

As shown in Fig. 21, it can be summarized that only the LLC was (nearly) exceeded. This means that spinal injuries are expected. According to different studies that analyzed glider accidents, over half of all injuries concern passengers' spines [5,38]. A runway crash comparable to the current crash test scenario occurred during the Shoreham Airshow in 2010, where the pilot also sustained spine injuries [39]. According to the test and simulation data, the protection of the spine plays a crucial role in increasing crash safety. Furthermore, the test showed an elevated risk of minor lower leg injuries in the proximity of the nose cone section, so these were marked in yellow.

Numerical loadcase studies

The crash model has been analyzed and validated for the load case of 15 m/s against a rigid barrier. The results facilitate a sound estimation of loadcases with deviating boundary conditions: Based on the validated model, two additional simulations were run where the initial velocity was raised to 20 m/s in one simulation and the barrier type was changed from a rigid to a deformable barrier.

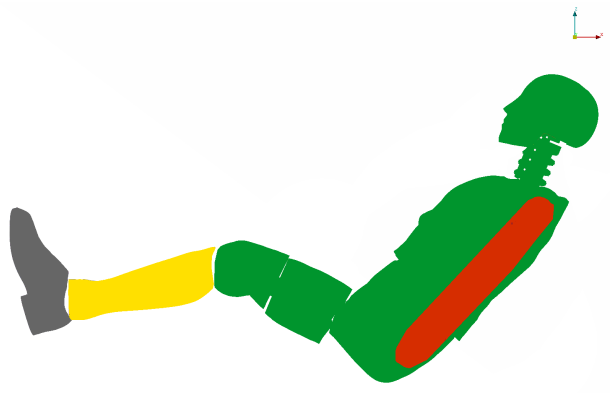

Fig. 21: Overview of the occupant's injury risks after a 15 m/s impact onto a rigid barrier based on the FEA results and validated by the test (green: low, yellow: moderate, red: high).

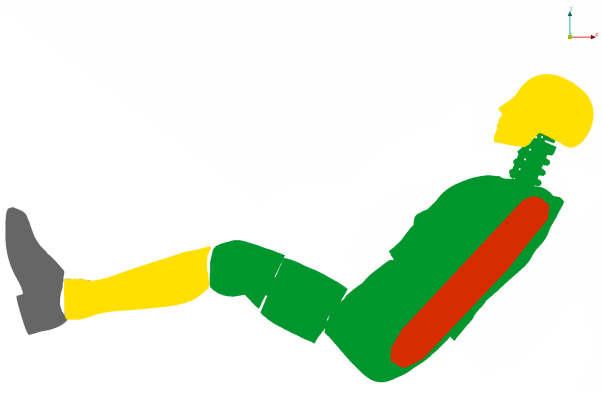

Fig. 23: Overview of the occupant's injury risks after a 20 m/s impact onto a rigid barrier based on the numerical study.

Study with 20 m/s impact velocity and rigid barrier

Figure 22 shows the simulation results of the variant with increased impact velocity 150 ms after the initial impact. It is shown that structural integrity is maintained even though the higher velocity results in a 78% increase in kinetic energy. Still, the fuselage exhibits the crushing failure mode, therefore, absorbs energy, protects the survival space behind it, and deflects the fuselage as intended. Nevertheless, it becomes clear that this loadcase is more critical for the pilot during the second impact: the rear fuselage reinforcement structure collapses during the tailslap. This creates high secondary loads onto the occupant, as shown in the next section.

As expected, the acceleration values are higher than the values oberseved during the impact with 15 m/s. The analysis of the Eiband curves shows that the limit values for slight injuries were exceeded in each case. An overview of the detailed evaluation of the local injury criteria is shown in Fig. 23. The HIC value is significantly higher but still uncritical, with a value of 181. However, a peak of 70 g occurs, which is close to the limit value of 80 g over 3 ms [35]. The head is therefore marked in yellow. The LLC is exceeded for this loadcase so back injuries are expected. The NIC values are below the injury limit. Consequently, the neck is colored green in the dummy overview diagram. Minor injuries are probable in the tibia region, so this area is colored yellow.

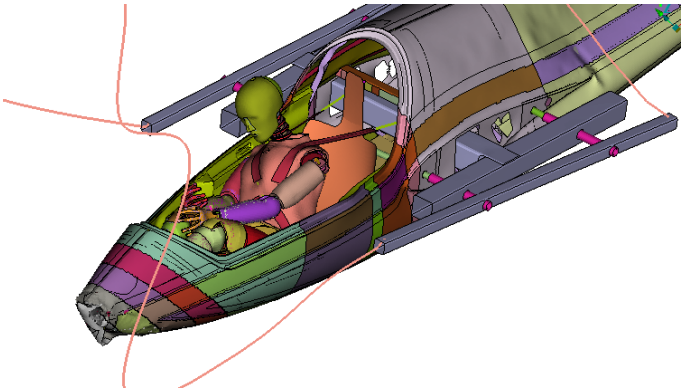

Fig. 22: Numerical study of an impact into a rigid barrier at 150 ms after the 20 m/s impact.

Study with deformable barrier

Possible accidents can take place over soft ground as well. Therefore, it is essential to investigate different ground conditions. A soil material model for soft, wet sand was used to investigate the crashworthiness of the fuselage impacting a deformable barrier [40, 41]. The optimization of the crash structure attempted to avoid digging into the ground and instead allow the structure to be deflected and subsequently slide along the ground. The desired behavior can be seen in Fig. 24, which shows the optimized behavior of the crash nose model.

The evaluation shows that the desired behavior could not be achieved. Unlike the reduced model, the nose of the fuselage digs into the soft ground. This can be clearly seen in Fig. 25, which shows the crash scenario 150 ms after the first impact. In contrast to the previous calculations, the fuselage decelerated nearly entirely in this short period. The accelerations indicate that this load case is hazardous for the occupant. Figure 26

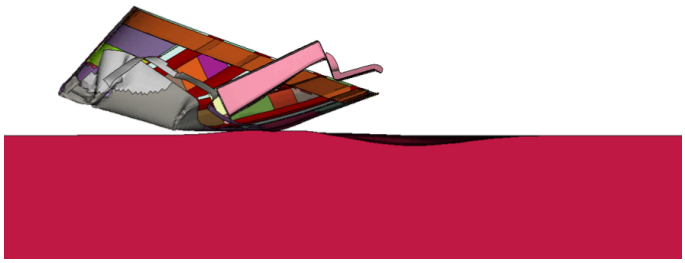

Fig. 24: Desired behavior of the nose cone of the fuselage at deformable barrier impact.

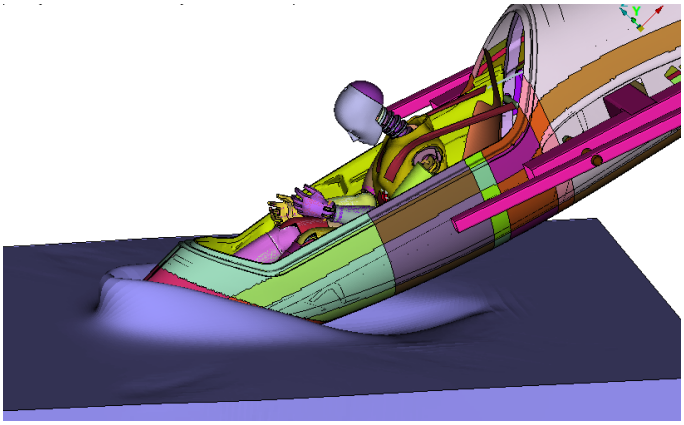

Fig. 25: Numerical study of an impact into a deformable barrier at 150 ms after the impact.

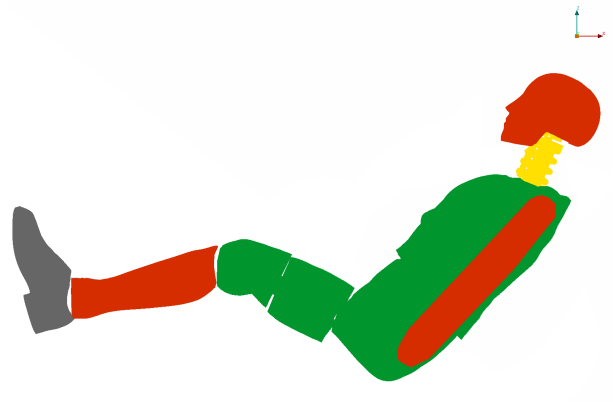

Fig. 26: Overview of the occupant's injury risks after a 15 m/s impact into a deformable barrier based on the numerical study.

shows an overview of the expected injuries. The head, neck and lumbar load criteria were exceeded. Therefore, the risk of injuries is significantly increased and the loadcase is estimated to be more critical than an impact onto a rigid barrier.

A possible reason for the difference between the intended nose cone failure and the behavior of the full-scale model can be found in the cohesive material model. The design and optimization were conducted with preliminary data, which were based on literature values and initial estimations. Subsequently, the crash kinematics of the fuselage changed significantly, which can be attributed to the increased stiffness of the fuselage structure. The difference between the simulations underlines the significance of reliable material data for the design process already in the pre-development phase.

Proposal of cockpit design methods

Improving the crashworthiness of a sailplane fuselage can be achieved by many approaches, which can occur with lightweight design and good manufacturability. Smooth transitions of the layup and the geometry maximize the possibility to absorb energy. Crash simulation models can be an effective tool to investigate and optimize an impacted structure, but it is not sufficient to simply reinforce and stiffen an existing structural design.

The approach of a stiff structure around the pilot provided by the reinforcement beams in combination with a continuously increasing laminate thickness from the nose tip toward the survival space showed promising results. This concept can be recommended as a baseline for future investigations. It is of high importance to adapt this solution to a specific structure to maximize crashworthiness.

Another option for future crashworthiness improvement is to increase the length of the fuselage front. At the same time, the crash structure must be compliant enough to absorb a considerable part of energy during the initial impact. These measures can have a positive effect on the further course of the crash. Additionally, the kinematics of the crash can be influenced, such that the maximum accelerations acting on the occupant are reduced considerably.

The evaluation of the injury criteria showed that spinal injuries are particularly critical. This was also confirmed by studies of Sperber, Lindner and an actual accident [5, 38, 39]. One way to reduce back injuries is to integrate an energy-absorbing structure into the seat shell. The project partner from Hannover integrated an energy-absorbing foam (Dynafoam) in the crash test, which was used as a cushion below the dummy. Critical lumbar loads were not surpassed in this test. Unfortunately, as of this writing there is no comparable full-scale test without such a cushion, that could have proven the effectiveness of this measure.

The present crash simulation model can be used as a baseline for developing future gliders or small engine planes. A simplified version of the model could also be used to optimize the crashworthiness iteratively. The evaluation of the injury criteria showed that the assessment based on accelerations provides a good indication of the injury severity of the pilot. As a consequence, essential estimates about the pilot's health can be made without a dummy. It should also be noted that the secondary impact (tailslap) has to be considered in the investigations of crashworthiness. Overall, the sizing of the composite fuselage provides a very good baseline for future fuselage optimization. The progressive increase in thickness of the structure described in section **Design of the Mü 32** is highly recommended. The Mü 32 design was not optimized for the tailslap loadcase. However, the reinforcement structure is significantly reduced after the cockpit opening towards the rear of the aircraft. Figure 3 shows the reduction in thickness of the reinforcement structure at a x-position of 2000 mm. The reduction in stiffness reduces the loads on the occupant after the secondary impact. Finally, the knowledge gathered from the CraCpit project should be used in the future, e.g. for crash design of urban air mobility concepts. Laarmann et al. presented a proposal for relevant eVTOL (Electric Vertical Take-Off and Landing aircraft) crash scenarios which show substantial equivalency to the proposed sailplane crash test [42]. The presented crash test and the simulation

model can be transferred to the development of eVTOLs efficiently. The material data have been published [43] and can be accessed via the authors of this paper and the Akaflieg Munich.

Conclusions

A novel sailplane cockpit design with reinforcement frames and a staggered layup in the nose cone section was described. A crash test setup was given based on accident analyses and an EASA certification specification. The crash design resulted in the desired failure mode of crushing to maximize energy absorption while sustaining a survival space around the pilot. The presented crash test setup is recommended for future crash investigations because the boundary conditions were satisfied in a reasonable range, which enabled detailed analysis of the crashworthiness and the validation of the crash simulation model.

Composite materials and an adhesive material were characterized in the scope of the present project. The obtained material properties, validated on several levels, are mandatory to build a high-quality simulation model. Small deviations of a single parameter in the material properties can have a significant impact in the failure behavior of the overall structure. The rope kinematics were included in the model and a physically reasonable friction coefficient was used between barrier and fuselage.

The fuselage was observed to be decelerated differently in the simulation than in the test. This difference was based on the velocity and acceleration curves. One possible reason is the limitation of LS-DYNA composite material model *MAT_058 which does not represent the rebound correctly. Consequently, the glider lifted off less from the ground than observed in the test after the first impact. Thus, acceleration loads in z-direction decreased, whereas the contact durations increased, leading to larger x-direction accelerations. As another consequence, the second impact occurs at a significantly earlier time than in the test. To further increase the quality of the crash model, a material model with plasticity formulation should be used. Furthermore, a parachute worn by the dummy could be integrated into the model. Also, the gravitational force of the dummy could be taken into account during the seating procedure to reach a more realistic dummy position.

The Eiband curves showed a reasonable estimation of the expected injuries. Thus, a simplified investigation of the occupant safety is possible without a crash dummy. However, a dummy is still necessary for detailed analysis of the estimated injuries as only the dummy is capable of predicting local injuries. The lumbar load was most critical for the occupant and should be closely scrutinized in future sailplane crashworthiness investigations. Also, numerical loadcase studies underlined the increased risk during impacts against deformable barriers or at elevated velocities.

Overall, the simulation model shows a good prediction of the full-scale sailplane crash test and underlines the maturity of today's numerical methods that are yet another step towards simulation-based certification in the future.

Acknowledgements

The authors would like to thank everyone who helped make the CraCpit project a great success. Furthermore, the support from Andreas Hoechbauer and Armin Gabler (BMW Group), Marco Mueller (MG Sensor), Thomas Lind and Sebastian Sauber (Me-Go GmbH), Bernd Voehringer (Imaging Solutions GmbH), Flugwerft Oberschleissheim and Treffler GmbH is highly acknowledged.

Funding

This work was funded by the project CraCpit (grant number 20E1703B) provided by the German Federal Ministry for Economic Affairs and Climate Action.

Declaration of conflicting interest

The authors declare that they have no known competing financial interests or personal relationships that might have influenced the work reported in this paper.

References

[1] Bundesstelle für Flugunfallforschung. Statistiken Flugunfälle und schwere Störungen, 2023/06/16. URL: `https://www.bfu-web.de/SiteGlobals/Forms/Suche/Statistikensuche_Formular.html`.

[2] European Union Aviation Safety Agency. *Certification specifications for sailplanes and powered sailplanes CS-22*. Amendment 1, 2008.

[3] Wolf Röger, Nieis Ludwig, and Manfred Conradi. Glider Ground Impact Tests. *Technical Soaring*, 23(4), 1999. URL: `https://journals.sfu.ca/ts/index.php/ts/article/view/376`.

[4] Gerhard Waibel. Designing a crashworthy cockpit sill: Proposal for an acceptable means of compliance according to OSTIVAS or JAR-22. *Technical Soaring*, 24(4), 2000. URL: `https://journals.sfu.ca/ts/index.php/ts/article/view/328`.

[5] Till Lindner. *Ermittlung eines Anforderungsprofils für den Entwurf von Sicherheitscockpits in Kleinflugzeugen und Bewertung möglicher konstruktiver Lösungen*. Seminar paper, Technical University of Braunschweig, 2019.

[6] Wolf Röger. *Safe and Crashworthy Cockpit*. FH Aachen, Fachbereich Luft-und Raumfahrttechnik, 2007.

[7] VDI guideline 5911. *Insassenschutz für Kleinflugzeuge*. 2022. URL: `https://www.vdi.de/richtlinien/details/vdi-5911-blatt-1-insassenschutz-fuer-kleinflugzeuge-flugzeugentwurf`.

[8] Christoph Kudla. *Auslegung und Detailkonstruktion des Rumpfes des Hochleistungs-Segelkunstflugzeugs Mü 32*. Bachelor thesis, Chair of Carbon Composites, Technical University of Munich, 2019.

[9] Uwe Schuster and Klaus Wolf. Improvement of sailplane crashworthiness through keel beams with silicone cores. *Technical Soaring*, 38(2):16–26, 2014. URL: https://journals.sfu.ca/ts/index.php/ts/article/view/529.

[10] Kevin Jeberien. *Entwicklung und FEM-gestützte Optimierung eines Energieabsorberkonzepts für Segelflugzeuge zur Steigerung der Unfalltauglichkeit*. Master thesis, Chair of Carbon Composites, Technical University of Munich, 2021.

[11] Joscha Loewe. *Konzeptionierung eines Crashtests an einer Segelflugzeugrumpfstruktur*. Bachelor thesis, Chair of Carbon Composites, Technical University of Munich, 2021.

[12] LS-Dyna. Livermoore Software. *LS-DYNA® KEYWORD USER'S MANUAL VOLUME II*.

[13] Anton Matzenmiller, Jacob Lubliner, and Robert L Taylor. A constitutive model for anisotropic damage in fiber-composites. *Mechanics of Materials*, 20(2):125–152, 1995. doi:10.1016/0167-6636(94)00053-0.

[14] Zvi Hashin. Failure criteria for unidirectional fiber composites. *Journal of Applied Mechanics*, 47:329–334, 1980. doi:10.1115/1.3153664.

[15] Karl Schweizerhof, Klaus Weimar, Thomas Munz, and Thomas Rottner. Crashworthiness analysis with enhanced composite material models in LS-DYNA – merits and limits. In *LS-DYNA world conference*, pages 1–17, 1998.

[16] Christian Pohl, Marco Toenjes, Christian Liebold, Marina Ploeckl, Hannes Koerber, Luciano Avila Gray, David Colin, and Klaus Drechsler. Numerical prediction of composite damage behavior: A modeling approach including the strain-rate-dependent material response. *Composite Structures*, 292:115628, 2022. doi:10.1016/j.compstruct.2022.115628.

[17] Christian Pohl, Huifang Liu, Daniel Thomson, Luciano Avila Gray, Drew E. Sommer, and Nik Petrinic. Dynamic crushing of composite coupons: An experimental and numerical study. *Journal of Composite Materials*, 57(26):4103–4121, 2023. doi:10.1177/00219983231201997.

[18] Stephan Marzi, Andrea Rauh, and Roland M Hinterhölzl. Fracture mechanical investigations and cohesive zone failure modelling on automotive composites. *Composite Structures*, 111:324–331, 2014. doi:10.1016/j.compstruct.2014.01.016.

[19] Marie Königbaur. *Validierung von Composite Materialkarten unter der Verwendung von 3-Punkt-Biege und Crushingversuchen*. Bachelor thesis, Chair of Carbon Composites, Technical University of Munich, 2022.

[20] Maria Lißner, Enrique Alabort, Borja Erice, Hao Cui, and Nik Petrinic. A rate dependent experimental and numerical analysis of adhesive joints under different loading directions. *The European Physical Journal Special Topics*, 227(1):85–97, 2018. doi:10.1140/epjst/e2018-00070-x.

[21] Sara Poxon. *The mechanical response of low to high density Rohacell foams*. PhD thesis, University of Oxford, 2013.

[22] Aase Reyes, Odd Sture Hopperstad, Torodd Berstad, Arve Grønsund Hanssen, and Magnus Langseth. Constitutive modeling of aluminum foam including fracture and statistical variation of density. *European Journal of Mechanics-A/Solids*, 22(6):815–835, 2003. doi:10.1016/j.euromechsol.2003.08.001.

[23] BETA CAE Systems. ANSA: Pre-Processing Suite. Accessed: 2024-07-07. URL: https://www.beta-cae.com.

[24] BETA CAE Systems. META: Post-Processing Suite. Accessed: 2024-07-07. URL: https://www.beta-cae.com.

[25] Xinran Xiao, Marc E. Botkin, and Nancy L. Johnson. Axial crush simulation of braided carbon tubes using MAT58 in LS-DYNA. *Thin-Walled Structures*, 47(6-7):740–749, 2009. doi:10.1016/j.tws.2008.12.004.

[26] Daniel M. Thomson, Borja Erice, Hao Cui, Justus Hoffmann, Jens Wiegand, and Nik Petrinic. A Puck-based localisation plane theory for rate- and pressure-dependent constitutive modelling of unidirectional fibre-reinforced polymers. *Composite Structures*, 184:299–305, 2018. doi:10.1016/j.compstruct.2017.09.088.

[27] The Executive Director Office Of The Federal Register Washington, D.C. Instrumentation for impact test. *SAE J211-1, Part 1, Electronic Instrumentation*, 1995.

[28] D. Cichos, D. de Vogel, M. Otto, O. Schaar, S. Zölsch, and D. Vetter. *Crash-Analyse, Beschreibung der Kriterien*, volume 2.1.1. Arbeitskreis Messdatenverarbeitung Fahrzeugsicherheit, Bundesanstalt für Straßenwesen, 2008.

[29] Harold M. Eiband. Human tolerance to rapidly applied accelerations: A summary of the literature. Technical Report NASA Memorandum 5-19-59E, National Aeronautics and Space Administration, Washington, D.C., 1959. URL: https://ntrs.nasa.gov/citations/19980228043.

[30] Dnenis F. Shanahan. Human Tolerance and Crash Survivability. In *Pathological Aspects and Associated Biodynamics in Aircraft Accident Investigation*. NATO RTO Educational Notes EN-HFM-113, 2004. URL: https://www.sto.nato.int/publications/STO%20Educational%20Notes/RTO-EN-HFM-113/EN-HFM-113-$$ALL.pdf.

[31] Julius Hoffelner. *Recherche zur Belastbarkeit des Menschen unter Crashlastfällen und Ableitung von Sicherheitsanforderungen an eine Segelflugzeug-Rumpfstruktur*. Semester thesis, Chair of Carbon Composites, Technical University of Munich, 2019.

[32] Dennis F. Shanahan. Pathological aspects and associate biodynamics in aircraft accident investigation. *RTO Educational Notes, EN-HFM-113*, 2004.

[33] John Hutchinson, Mark J. Kaiser, and Hamid M. Lankarani. The head injury criterion (HIC) functional. *Applied mathematics and computation*, 96(1):1–16, 1998. doi:10.1016/S0096-3003(97)10106-0.

[34] Murray Mackay. The increasing importance of the biomechanics of impact trauma. *Sadhana*, 32(4):397–408, 2007. doi:10.1007/s12046-007-0031-9.

[35] Kai-Uwe Schmitt, Peter F. Niederer, Duane S. Cronin, Barclay Morrison III, Markus H. Muser, and Felix Walz. *Trauma Biomechanics*. Springer, 2019.

[36] Department of Defense, United States of America. *Joint service specification guide - crew systems crash protection handbook*. 1998.

[37] Anthony Segal. Pilot Safety and Spinal Injury. *Technical Soaring*, 12(4), 1988. URL: https://journals.sfu.ca/ts/index.php/ts/article/view/801.

[38] Martin Sperber. Untersuchung des insassenschutzes bei unfällen mit segelflugzeugen und motorseglern. *TÜV Rheinland Kraftfahrt GmbH, Forschungsbericht L-2/93-50112/92 on behalf of the German Ministry of Transport*, 1998.

[39] AAIB Field Investigation. AAIB Bulletin. 7:47–56, 2011.

[40] Michael A. Thomas, Daniel E. Chitty, Martin L. Gildea, and Casey M. T'Kindt. *NASA/CR-2008-215334: Constitutive Soil Properties for Unwashed Sand and Kennedy Space Center*. 2008. URL: https://ntrs.nasa.gov/citations/20080032551.

[41] Ernest Heymsfield, Edwin L. Fasanella, Robin C. Hardy, and Richard L. Boitnott. Assessment of soil modeling capability for orion contingency land landing. *Journal of Aerospace Engineering*, 25(1):125–131, 2012. doi:10.1061/(ASCE)AS.1943-5525.0000089.

[42] Lukas Laarmann, Andreas Thoma, Philipp Misch, Thilo Röth, Carsten Braun, Simon Watkins, and Mohammad Fard. Automotive safety approach for future evtol vehicles. *CEAS Aeronautical Journal*, 14:369–379, 2023. doi:10.1007/s13272-023-00655-0.

[43] Christian Pohl. *Übersicht Materialkennwerte LuFo-Projekt CraCpit*. Chair of Carbon Composites, Technical University of Munich, 2022.